Cosine Error-Free Metrology Tool Path Planning for Thickness Profile Measurements

Xiangyu Guo
J. Mike Walker
'66 Department of Mechanical Engineering,
Texas A&M University,
3123 TAMU,
College Station, TX 77843-3123
e-mail: xiangyug33@tamu.edu

ChaBum Lee[1]
J. Mike Walker
'66 Department of Mechanical Engineering,
Texas A&M University,
3123 TAMU,
College Station, TX 77843-3123
e-mail: cblee@tamu.edu

This paper presents a novel thickness profile measuring system that measures double-sided thin pipe wall surfaces in a non-contact, continuous, cosine error-free, and fast manner. The surface metrology tool path was developed to align the displacement sensors always normal to the double-sided surfaces to remove cosine error. A pair of capacitive-type sensors that were placed on the rotary and linear axes simultaneously scans the inner and outer surfaces of thin walls. Because the rotational error of the rotary axis can severely affect the accuracy in thickness profile measurement, such error was initially characterized by a reversal method. It was compensated for along the rotational direction while measuring the measurement target. Two measurement targets (circular and elliptical metal pipe-type thin walls) were prepared to validate the developed measurement method and system. Not only inner and outer surface profiles but also thin-wall thickness profiles were measured simultaneously. Based on the output data, the circularity and wall thickness variation were calculated. The thickness profile results showed a good agreement with those obtained by a contact-type micrometer (1-μm resolution) at every 6-deg interval. The uncertainty budget for this measuring system with metrology tool path planning was estimated at approximately 1.4 μm. [DOI: 10.1115/1.4048433]

Keywords: profile measurement, thickness measurement, non-contact, cosine error, capacitive-type sensors, inspection and quality control, metrology

1 Introduction

Apart from the metrology of the surface profile, thickness profile measurement is also a critical technology in process control and quality assurance for checking the geometry dimensions of surface conditions of pipes, bearings, or tubes. Such thickness metrology techniques using dimensional measuring sensors have been used in many industrial applications. Because of the uniqueness or measuring principles of each measurement system, there exist a few types of measurement methods such as non-contact/contact, single-sided/double-sided thickness, and non-destructive/destructive measurement methods [1].

The contact method is easy to operate and can offer direct profile or thickness information. The most commonly applied approaches are thickness gages and coordinate measurement methods (CMM). However, their measurement location, speed, and accuracy are limited. Many non-contact methods have been developed to overcome those limitations. Monchalin et al. [1,2] proposed a method for mapping the tube thickness using ultrasonic and optical displacement sensors. The location of defects on the tube was first detected, and the surface quality was analyzed focusing on the detected area. Yi [3] evaluated the performance of an ultrasonic method for the number of flaws in pipe wall detection. Belenkij et al. [4] claimed a method using the X-ray technique to measure the inner and outer sides of the tube. Thus, the thickness could be calculated. Mao and Lei [5] put forward a method to estimate the thickness of the pipe using swept-frequency eddy current testing along with the Levenberg–Marquardt algorithm. Those methods are efficient but are relatively expensive and limited to the measurement targets and testing conditions. A majority of research using optical methods was developed, those investigations usually target the transparent, metallic, oil, and aerostatic thin-film layers coated or deposited on the base layer. Kim and Kim [6] and Ghim and Kim [7] developed thin-film metrology using white-light interferometry, while Xie et al. [8] applied structured illumination microscopy on the transparent thin-film measurement. Other methods based on the spectroscopic ellipsometry, which was proposed by Jellison et al. [9], and Fresnel diffraction, which was brought up by Hassani and coauthors [10,11], were also developed. When it comes to the metal thin-wall thickness measurements, it is not appropriate due to the high requirement for the alignment and testing environment. Still, there are few studies on measurement technology for obtaining continuous thickness profiles in a single measurement activity as well as for eliminating cosine error.

Guo et al. [12] introduced the discrete cosine error-free surface measurement technique utilizing the precision spindle with a single capacitive sensor. This method can successfully provide both of the inner and the outer spherical surface profile information discretely. Although the thickness could be calculated by measured surface profile information, it could not precisely present the thickness profile as it is challenging to match the measurement point between the inner and outer surface to be at the same location. In general, double-sided simultaneous thickness profile measurement techniques show advantages regarding accuracy, precision, and measuring speed, as the error from the coordinate mismatch of the inner and outer sides can be ignored.

Cosine error in surface profile measurement comes from an angular misalignment between the measurement axis and the axis of motion, and this error negatively affects the measurement accuracy [12,13]. For flat surface measurement, the cosine error could be compensated easily after the testing process because it generates a constant difference between the actual value. In measuring nonplanar surface, like the spherical, aspherical, or freeform surfaces, because the axis of measurement changes all the time, the negative effect from cosine error may be inevitable. Many previous studies have introduced the cosine error compensation methods [13], but there are few research pieces about eliminating cosine error during the measurements.

Capacitive sensing based on the capacitive coupling is a technology that can detect and measure anything that is conductive or has a dielectric constant different from the air. As the object being sensed moves a distance from the electrodes, the capacitance changes.

[1]Corresponding author.
Manuscript received March 27, 2020; final manuscript received August 30, 2020; published online October 27, 2020. Assoc. Editor: Dragan Djurdjanovic.

Capacitive sensors (CSs) have been widely used in displacement measurement applications for many decades [14]. The typical applications are distance [15], location [16], and surface profiling, like the surface roughness parameters [17]. Unlike other non-contact displacement sensors, CSs offer many desirable properties, e.g., low cost, low energy consumption [18], flexible and variable structure design, and fit with different environments. However, the linear detection range of a CS is dependent on the sensing area, probe/electrode shape, target size, and driver as well; resolution and sensitivity rely on the same conditions as a detection range [19].

In this study, a thickness and profile measurement system, which is a double-sided continuous cosine error-free measurement technique, is discussed. For eliminating the cosine error, the displacement probes are always required to be aligned normal to the measurement target surfaces. Toward that, a pair of capacitive sensors was installed facing each other with offset distance measuring the target inner and outer surfaces synchronously, and a tool path planning method was discussed to improve the alignment quality between the sensor probes and target surface. Apart from the circular targets, the tool path planning methods also allow this technique to be applied with elliptical surface.

2 Measurement Principle

2.1 Cosine Error Elimination Method. As shown in Fig. 1, for the circular target surface measurement, only the spindle motion was activated, and the spindle and linear axes were used for elliptical target surface measurement. As ideally, an invariable constant radius of curvature (RoC) exists along the periphery for both inner and outer surface profiles. For the elliptical target, the difference exists between the length of the major and minor axis; the RoC changes along the periphery, so the linear motion axis was added. The centers of the artifact and target samples were overlapped for both cases, while CSs were placed along the spindle rotational axis. The starting-point position can be anywhere when measuring the circular target. However, this starting location should be aligned with either the minor or the major axis under the test of the elliptical target for straightforward measurement path calculation. The initial displacement between both CSs and the target surfaces at the starting-point was set to be the same.

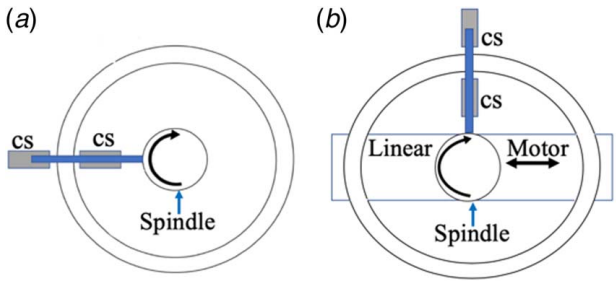

Fig. 1 The relationship between the target and the sensors when measuring the (*a*) circular target and (*b*) the elliptical target

2.2 Metrology Tool Path Planning. In the proposed non-contact, continuous, cosine error-free thickness measurement system, the scanning tool path for the circular metal target is obvious. Once one cycle of rotary scanning ends, the measurement is finished. Both inner and outer surface information can be simultaneously collected. On the other hand, the case for the elliptical metal thin-wall pipe sample is different. Since this thickness measurement is a double-side synchronous process, we take an example of the internal moving orbit scanning process. The schematic description for the corresponded path design process is given in Fig. 2. The θ_i and x_i are the spindle rotating angle and linear motor's moving distance from the starting-point o to point i. The lengths of the semi-major and minor axis are a and b individually. The d_0 is the original offset between CS and the target surface, and d_i can be expressed by:

$$d_i = d_0 + \Delta d_i \tag{1}$$

where Δd_i is the deviation from d_0 at point i.

Under the polar coordinate system, the inner surface scanning motion orbit composed by point i (X_i, Y_i) can be written from the ellipse equation:

$$f(X_i, Y_i) = \frac{X_i^2}{(a-d_0)^2} + \frac{Y_i^2}{(b-d_0)^2} - 1, \quad \text{and } f(X_i, Y_i) = 0 \tag{2a}$$

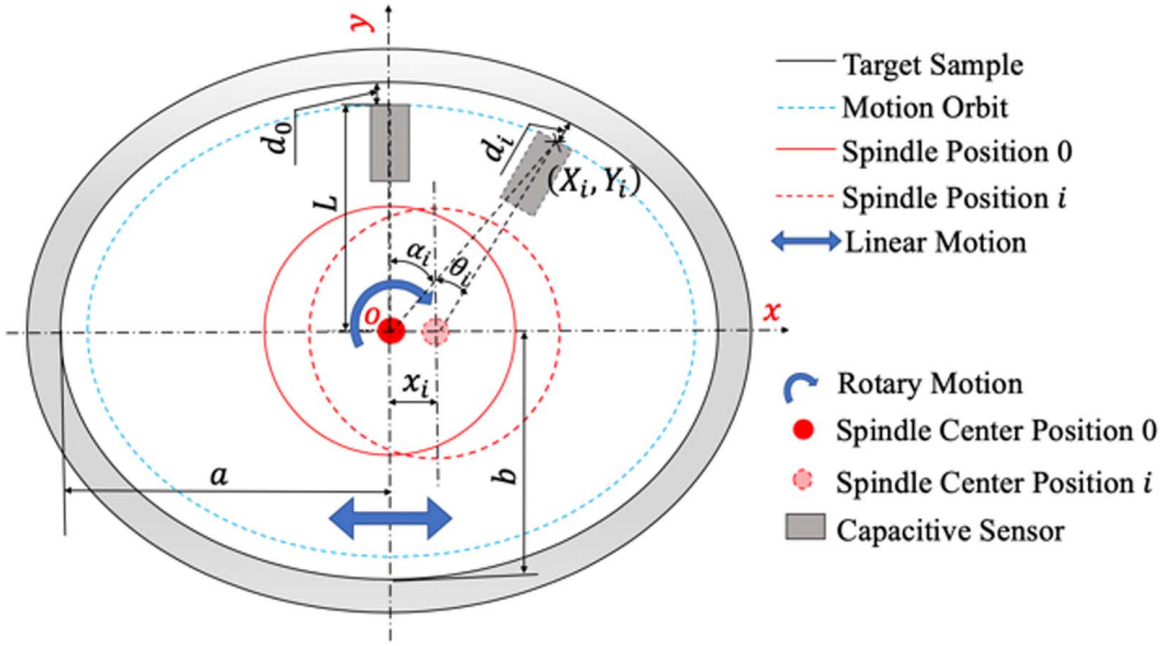

Fig. 2 Metrology tool path planning process for the elliptical target surface measurement

$$X_i = (a - d_0) \cdot \sin(\alpha_i) \tag{2b}$$

$$Y_i = (b - d_0) \cdot \cos(\alpha_i) \tag{2c}$$

Here, L is the length from the center of the spindle to the edge of the CS, which is also the length of the artifact's arm that supports the CSs, which can be measured from the caliper. The equation above can be transferred into

$$X_i = (a - b) \cdot \sin(\alpha_i) + L \cdot \sin(a_i) \tag{3a}$$

$$Y_i = L \cdot \cos(\alpha_i) \tag{3b}$$

where $L = b - d_0$

As the spindle system provides the motion for $L \cdot \cos(\alpha_i)$ and $L \cdot \sin(\alpha_i)$, from above, the linear motor's moving distance x_i is

$$x_i = (a - b) \cdot \sin(\alpha_i) \ (i = 0, 1, 2, \ldots) \tag{4}$$

Since CSs should be faced normal to the target of each other, the practical scanning rotation θ_i was set by the reciprocal of the differential of the target surface profile from point to point. It is worth noting that the range for θ_i changes from 0 deg to 360 deg when transferring the data into angles, and the end position of θ_i was set as 360 deg. The relationship between the rotation angle and coordinates can be expressed as

$$\begin{aligned} \tan(\theta_i) &= \frac{\Delta X_i}{\Delta Y_i} = \frac{1}{f'(X_i, Y_i)} (i = 0, 1, 2, \ldots) \\ &= \left(\frac{a - b}{L} + 1 \right) \cdot \Delta \tan(\alpha_i) \end{aligned} \tag{5}$$

The size of the targets determines the measurement time. A G-code language was applied to achieve such metrology tool path planning for x_i and θ_i, and the measured data for both CSs were collected continuously in phase.

3 Experiment Background

3.1 Experiment Setup and Target Sample Information. An aerostatic bearing spindle and linear axes were utilized in the experiment. A pair of CSs were placed on the artifact of the aerostatic bearing spindle along with the rotation axis, which offered the rotary motion. When using a pair of CSs as displacement sensors simultaneously, the master–slave mode was applied. In case the potential electrical interference exists between each sensor. The sensitivity of each CS toward the target was calculated. The corresponded effective sensing area was with a diameter of 3 mm, and the near gap range was 0.5 mm. A sensor jig structure was designed and manufactured to ensure that the pair of CSs measures the same area on both sides. Two aluminum structures for each CS were connected by a set screw, the centered holes were drilled with the same diameter of CSs at the same position, and the position adjusting bar was connected with the sensor jig. The linear axis was linked to the spindle system to further assisting the non-circular target's measurement. The overall mechanical setup, the installation of the CSs, as well as the sensor jig schematic are presented in Fig. 3.

The information of target samples is described below. In the presented experiment study, the technical data for the target surface profile like RoC and (a) the length of semi-major and (b) minor axis for elliptical pipe were treated as ideal. Figure 4 shows the (a) circular and (b) elliptical target for this study.

The provided geometry data of the target samples are listed in Table 1.

3.2 Spindle Error Separation. The spindle rotational error $S(\theta)$ was separated from the part (artifact) error $R(\theta)$ by a reversal method proposed by Bryan [20] and Donaldson [21]. The artifact and CS were placed at an arbitrary angular position on the spindle, and a roundness trace $m_1(\theta)$ was acquired from one of the CS. Then, both the CS and the artifact were rotated both 180 deg, traced the roundness again, and $m_2(\theta)$ was measured. The relationship between $S(\theta)$, $R(\theta)$, $m_1(\theta)$, and $m_2(\theta)$ is shown below

$$S(\theta) = m_1(\theta) - m_2(\theta) \tag{6}$$

$$R(\theta) = m_1(\theta) + m_2(\theta) \tag{7}$$

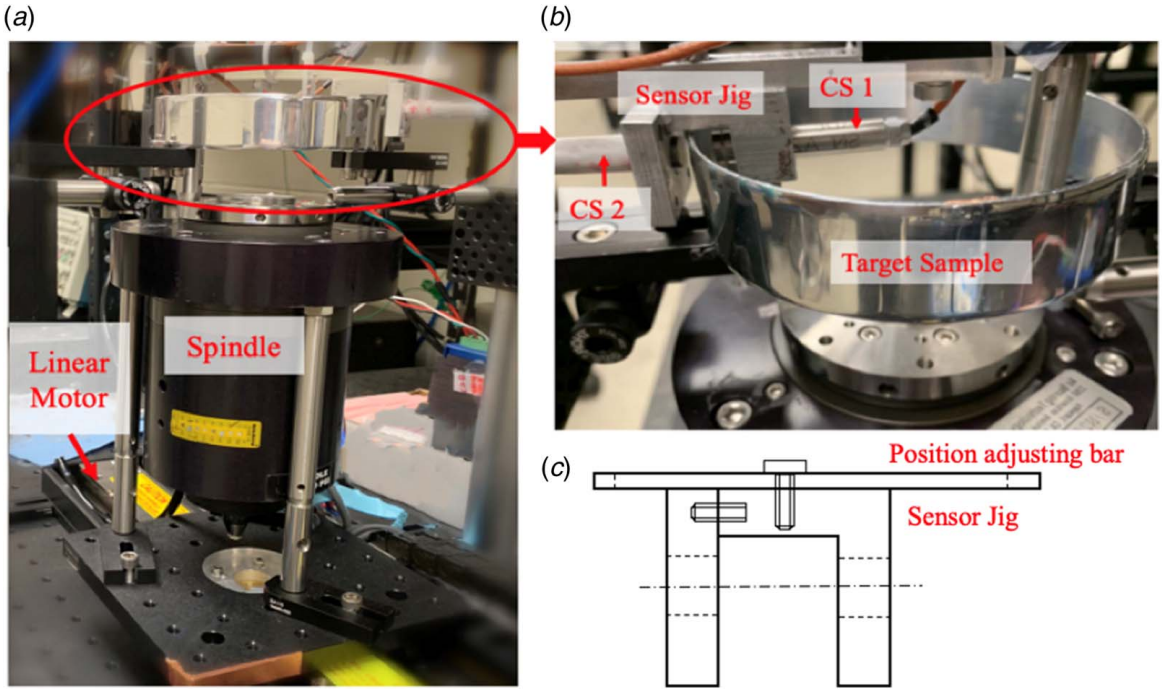

Fig. 3 (a) Proposed thickness profiling system, (b) the installation of CSs, and (c) the schematic of CSs jig

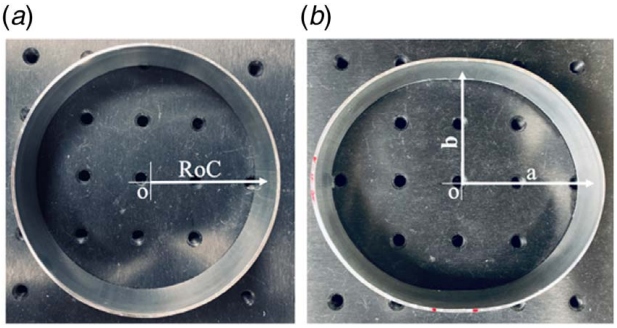

Fig. 4 (*a*) Circular and (*b*) elliptical target sample

Table 1 Surface profile information for circular and elliptical metal target samples

	RoC (mm)		a (mm)		b (mm)	
	Inner	Outer	Inner	Outer	Inner	Outer
Circular target	48.9	50.8	–			
Elliptical target	–		52.1	54.1	45.0	47.0

The results are shown in Fig. 5. The root-mean-square (RMS) value for the spindle error $S(\theta)$ was 0.031 μm, and its peak-to-valley (PV) value was 0.136 μm.

3.3 Calculation of Surface and Thickness Profiles. The dominant distance from the target center to the target surface is d_0, and the sensor output is $d_i(\theta)$. Thus, the surface profiles $P(\theta)$ can be expressed as

$$P(\theta) = d_0 + \Delta d_i(\theta) - s(\theta) \tag{8}$$

where $\Delta d_i(\theta) = d_i(\theta) - d_0$

Once we acquire both inner $P_i(\theta)$ and outer surface profiles $P_o(\theta)$, the thickness distribution T(θ) along each rotary angle can be expressed as

$$T(\theta) = P_o(\theta) - P_i(\theta) \tag{9}$$

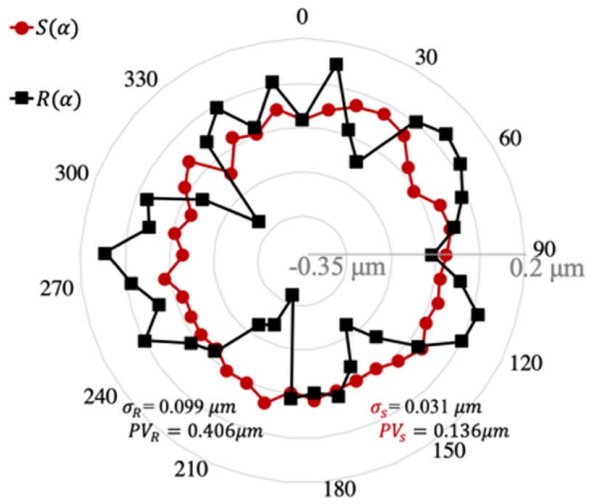

Fig. 5 Spindle error separation by reversal method

4 Experiment Results Comparison

4.1 Surface Profiles Comparison. Figure 6 compares the ideal and the average measured surface profiles in both sides of the circular and elliptical metal sample, where the offered RoC generates the ideal surface profiles for circular sample or (a) and (b) for the elliptical metal sample. The circularity is a form of tolerance, and it means that all points of the surface intersected by a plane perpendicular to an axis or spine (curved line) are equidistant from that axis or spine [22]. The tolerance zone is the area between two coaxial circles, which is the radius distance between the minim and maximum deviation from the measurement results [23].

The circularity tolerance for the inner and outer surfaces under the case of the circular sample was 0.427 mm and 0.526 mm, respectively. For the elliptical target, there is no established standard for the ellipticity. However, the ellipticity measurement process has been defined and studied in the literature [24]. The ellipticity measures how much a shape considered differs from a perfect ellipse [25]. To keep the consistency with circularity, we define the ellipticity tolerance zone as the area between two coaxial ellipses so that the tolerance for the inner and outer surface is under the case of the elliptical sample was 0.417 mm and 0.572 mm.

4.2 Thickness Profile Comparison. Thickness results were consistent throughout each of the three repeated experiments by the proposed technique. A contact-type electronic micrometer (from MITUTOYO) with 1-μm resolution was used as the baseline comparison sensor; it collected the thickness information at every 6 deg along with the profiles where CSs measured. In the same way, three repeated measurements were performed for the contact measurement. By extracting a similar measured point from the continuous thickness measurement method to match the micrometer's gathered data, the thickness values collected by both methods were also compared. The maximum deviation was at 312 with 15.2 μm (0.8%) for circular target, and other measured points deviations were within 5 μm (0.2%). For the elliptical target, the maximum deviation was at 186 with −22.3 μm (1%), and other measured points deviations were within 10 μm (0.5%). Figure 7 presents the thickness distribution and the calculated deviation comparison; here, the micrometer's results are the averaged results from three times measurements.

The thickness on average and standard deviation of the circular target was 1.877 mm and 0.062 mm individually, and the elliptical target is 1.941 mm and 0.109 mm.

In the tube system, their walls thickness uniformity is important, and any variation in wall thickness would indicate such tolerance [26]. The thickness variation V can be calculated by the equation is shown below.

$$V = \frac{T_{\min}}{T_{\max}} \times 100\% \tag{10}$$

The thickness variation for the circular and elliptical sample was estimated at 91.34% and 80.95% separately. Thus, it was confirmed that the non-contact cosine error-free continuous double-side thickness profilometer could measure the target profiles, thickness, and calculate geometry tolerance like circularity and thickness uniformity.

5 Uncertainty Analysis

Four primary uncertainty sources were considered for the proposed thickness measurement technique: instrumentation, installation, environment, and axis-motion quality.

5.1 Instrumentation Uncertainty. The instrumentation uncertainty comes from the noise level of the pair of CSs. The pair of CSs was set at the initial measurement location, and three comparisons were made in Fig. 8. Motor-on or motor-off indicates

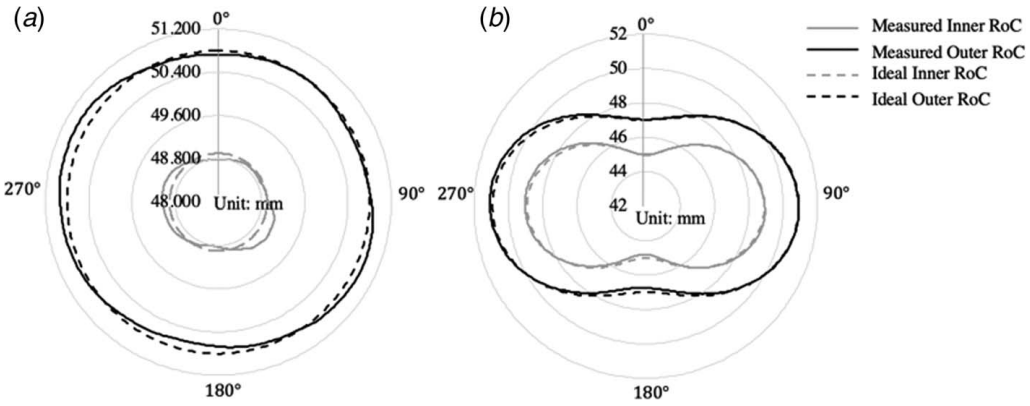

Fig. 6 (*a*) Circular and (*b*) elliptical metal thin-wall pipe surface profiles comparison

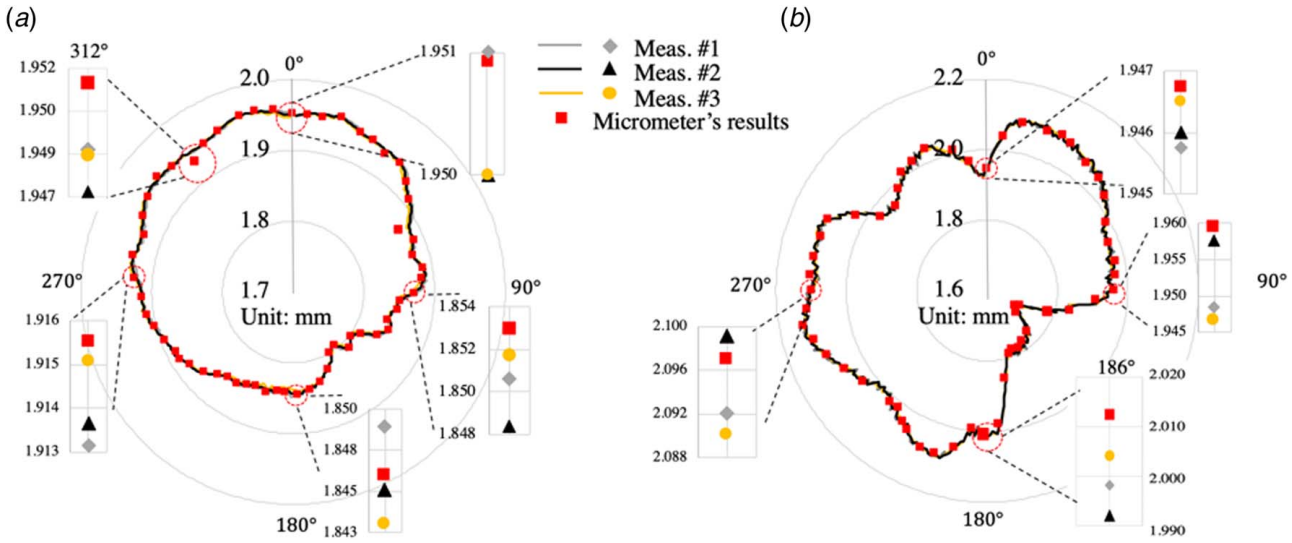

Fig. 7 Thickness deviations between contact micrometer and proposed profilometer: (*a*) circular target and (*b*) the elliptical target results

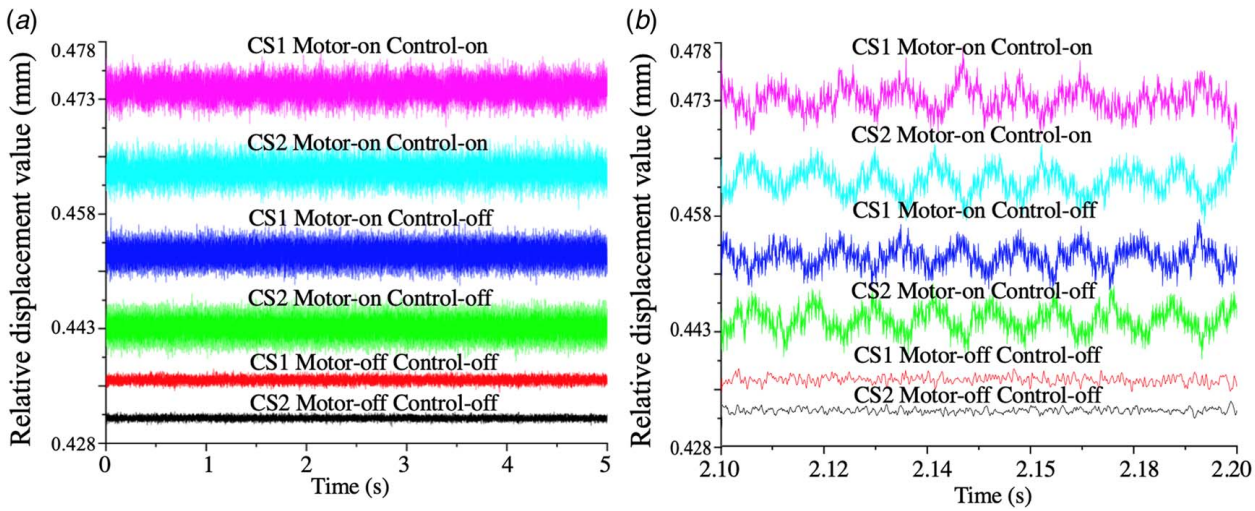

Fig. 8 Noise-level comparison in both CSs under three cases for (*a*) continuously measured in 5 s and (*b*) from 2.10–2.20 s

Table 2 Noise level for three cases

	Motor-off/ control-off	Motor-on/ control-off	Motor-on/ control-on
Noise level (μm)	0.3	0.8	0.8

both rotary and linear axis motors were on or off. Control-on or off indicates that the controller system was on or off work. The sampling rate was 10 kHz.

As the pair of CSs were placed face to face along the spindle rotation axis, the direction for the collected noise was opposed. The noise level (N) for each situation in this system can be calculated by the equation below:

$$N = \mathrm{RMS}\left(\frac{O_1}{S_1} + \frac{O_2}{S_2}\right) \tag{11}$$

Here, O_1 and O_2 are the output (mv) of each CS, and S_1 and S_2 are the sensitivity of matched CS. Table 2 presents the noise level for each case. The control-on and motor-on is the case for the performed experiment.

5.2 Installation Uncertainty. The error from using a conventionally calibrated CS with a non-flat target is typically neglected unless the research is to reach nanometer-level accuracy [27]. CS measures the electric potential obtained from averaging the active sensing area between measuring probe and target surface. By principle, there is a measurement error when measuring non-flat target surfaces such as curved surfaces. In the experiment, the sensor-effective sensing area is relatively small compared to the radius of the target surface's curvature. Here, we did not include the measurement area error of CSs.

The installation error was shown in Fig. 9. These alignment uncertainties can affect the measured surface profile's accuracy. These uncertainties can be minimized for the thickness measurement, as the pair of CSs were in the same line and faced opposite each other.

Based on Fig. 9, the experiments were set for the offset as ± 100 μm and angular deviation as ± 5 deg for the surface profiles. The corresponded effects are in Table 3.

5.3 Environmental Uncertainty. The lab temperature was stable at 23 °C with ±1 °C temperature variation. Compressed air was regulated for the spindle system, and a vibration-isolated granite table was applied for the experiment setup. Humidity variation was not considered. The Capacitec (CS manufacturer) analyzed the thermal drift effect for the sensor [28]. The aerostatic bearing spindle, as well as the linear axis, is also affected from the thermal drift, and Tan et al. [29] investigated into those influences. Those uncertainty values were found from the references and presented in Table 4.

Table 3 Installation uncertainty effects on surface profiles measurement

	Probe offset	Probe angular misalignment	Target positioning error
Noise level (μm)	0.47	0.78	0.48

Table 4 Thermal drift uncertainty

Sensor	Spindle	Linear axis
$u_{E1} = 80$ ppm/°C [28]	$u_{E2} = 90$ ppm/°C [29]	$u_{E3} = 90$ ppm/°C [29]

5.4 Axis-Motion Quality. The spindle axis quality was presented in Sec. 4, where the spindle error and the part error have been separated and calculated. The linear axis quality is how accurate the linear motion can be operated. Setting a CS toward the linear motion direction, the performance of 100 μm linear moving motion under three cases was studied. Figure 10 shows the results of the uncertainty at the stationary state after 100-μm movement were achieved. The rotary motion-on was the experiment circumstance, and the related RMS value was 0.6 μm. However, this uncertainty will not affect the thickness measurement results because of the mechanical setup structure for the pair of CSs.

Together, the measurement uncertainty of the proposed system was budgeted below, the measurement uncertainty of the proposed thickness profile measuring system by the measurement limits at a given confidence level (95% confidence, $k = 2$ (Table 5)).

6 Conclusion

A non-contact, continuous, cosine error-free thickness profile measurement method for double-sided thin-wall structures (circular and elliptical targets) was proposed and validated by the traditional measurement method, which is the micrometer measurement. The metrology tool path planning to fundamentally avoid cosine error for circular and elliptical thin-wall profile measurements was developed. Because well-planned computer numerical control (CNC) tool paths by compensating for volumetric error can significantly increase the machining efficiency, the proposed metrology tool path planning for surface profiles and thickness can improve measurement speed, precision, accuracy, and uncertainty by eliminating cosine error. Two separated and three-times repeated experiments on circular and elliptical targets were presented. Both inner and outer surface profiles were measured, and the subtracted thickness profiles were compared with contact-type micrometer every 6 deg, most of the deviations were within 5 μm (0.2%) and 10 μm (0.5%). The repeated experiment results were consistent with those of the baseline comparison sensor, which indicates that the proposed metrology path planning for the thickness profile has the potential for arbitrary three-dimensional surface metrology

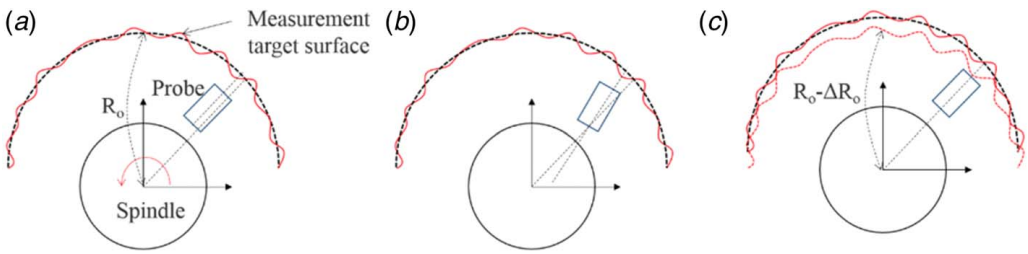

Fig. 9 Measurement uncertainty sources (alignment errors): (*a*) probe offset error, (*b*) probe angular alignment error, and (c) target positioning error [12].

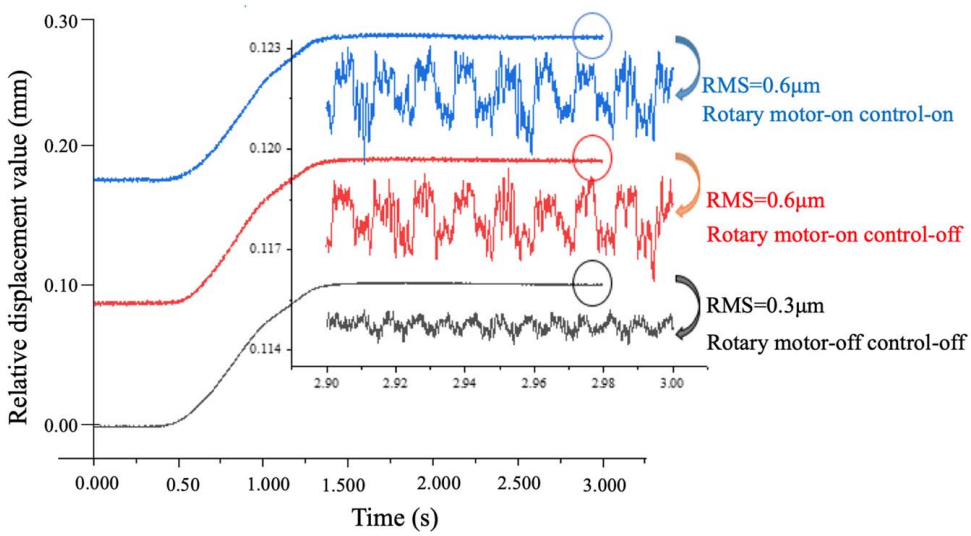

Fig. 10 Linear motion performance evaluation under three cases

Table 5 The proposed profilometer's uncertainty budget

Uncertainty source	Details	Uncertainty (μm)
Instrumentation error	(Fig. 8)	0.8
Installation error [12]	Probe offset error	0.47
	Probe angular error	0.78
	Target positioning error	0.48
Environmental error	Thermal drift (sensor) [28]	0.008
	Thermal drift (spindle) [29]	0.009
	Thermal drift (linear axis) [29]	0.009
	Compressed air pressure regulated	
	Ground vibration-isolated environment	
Axis motion quality	Spindle error (Fig. 5)	0.031
	Linear axis error (Fig. 10)	0.6
Total uncertainty	95% confidence level ($k = 2$)	1.4

accurately and precisely. The related uncertainty budget was estimated to be 1.4 μm.

However, as the tool path planning method is based on the assumption that the information on the original target sample is perfect, if the initial data are not perfect, cosine-error would still be brought into the results, as shown in Fig. 9(*c*). Besides, the measurement resolution in the axial and lateral directions was limited due to the sensor's measuring range and effective sensing area. The choices of sensors should be optimized for the measurement targets to increase the resolution in the axial and lateral directions. Besides, to allow this technique suitable for various target samples, the metrology tool path planning combined with high precision multi-axis positioning control algorithms must be developed to enable the three-dimensional thickness profile measurements.

Acknowledgment

The research was supported by the National Science Foundation (Award Number: CMMI 1663210) through the Texas A&M University, and the authors would like to thank Dr. Joshua A. Tarbutton at University of North Carolina at Charlotte for valuable comments.

Data Availability Statement

The data sets generated and supporting the findings of this article are obtainable from the corresponding author upon reasonable request. The authors attest that all data for this study are included in the paper.

References

[1] Monchalin, J. P., Blouin, A., and Padioleau, C., 1999, Method and Apparatus for Mapping the Wall Thickness of Tubes During Production, US607839A.
[2] Monchalin, J. P., Blouin, A., and Padioleau, C., 1999, Apparatus for mapping the wall thickness of a tube or other object having movement in two directions, BR0009831A.
[3] Yi, W.-G., Lee, M.-R., Lee, J.-H., and Lee, S.-H., 2006, "A Study on the Ultrasonic Thickness Measurement of Wall Thinned Pipe in Nuclear Power Plants," Paper Presented at the 12th Asia-Pacific Conference on NDT, Auckland, New Zealand, Nov. 5–10,
[4] Belenkij, J., Müller, C., and Scharmach, M., 2000, "A new Method for Radiographic Image Evaluation for Pipe Wall Thickness Measurement," 15th World Conference on Nondestructive Testing, Roma, Italy, Oct. 15–21.
[5] Mao, X., and Lei, Y., 2016, "Thickness Measurement of Metal Pipe Using Swept-Frequency Eddy Current Testing," NDT&E Int., **78**, pp. 10–19.
[6] Kim, S.-W., and Kim, G.-H., 1999, "Thickness-Profile Measurement of Transparent Thin-Film Layers by White-Light Scanning Interferometry," Appl. Opt., **38**(28), pp. 5968–5973.
[7] Ghim, Y.-S., and Kim, S.-W., 2006, "Thin-Film Thickness Profile and Its Refractive Index Measurements by Dispersive White-Light Interferometry," Opt. Express, **14**(24), pp. 11885–11891.
[8] Xie, Z., Tang, Y., Zhou, Y., and Deng, Q., 2018, "Surface and Thickness Measurement of Transparent Thin-Film Layers Utilizing Modulation-Based Structured-Illumination Microscopy," Opt. Express, **26**(3), pp. 2944–2953.
[9] Jellison, G., Jr., Modine, F., Doshi, P., and Rohatgi, A., 1998, "Spectroscopic Ellipsometry Characterization of Thin-Film Silicon Nitride," Thin Solid Films, **313**, pp. 193–197.
[10] Hassani, K., Ashrafganjoie, M., and Tavassoly, M. T., 2016, "Application of White Light Fresnel Diffractometry to Film Thickness Measurement," Appl. Opt., **55**(7), pp. 1803–1807.
[11] Tavassoly, M. T., Haghighi, I. M., and Hassani, K., 2009, "Application of Fresnel Diffraction From a Phase Step to the Measurement of Film Thickness," Appl. Opt., **48**(29), pp. 5497–5501.
[12] Guo, X., Han, J., and Lee, C., 2020, "Cosine Error Elimination Method for One-Dimensional Convex and Concave Surface Profile Measurements," ASME J. Manuf. Sci. Eng., **142**(4), p. 041001.
[13] Leach, R., 2014, *Fundamental Principles of Engineering Nanometrology*, Elsevier, New York.
[14] Ye, Y., Zhang, C., He, C., Wang, X., Huang, J., and Deng, J., 2020, "A Review on Applications of Capacitive Displacement Sensing for Capacitive Proximity Sensor," IEEE Access, **8**, pp. 45325–45342.
[15] Barile, G., Ferri, G., Parente, F. R., Stornelli, V., Sisinni, E., Depari, A., and Flammini, A., 2018, "A CMOS Full-Range Linear Integrated Interface for Differential Capacitive Sensor Readout," Sens. Actuators, A, **281**, pp. 130–140.

[16] Arshad, A., Khan, S., Zahirul Alam, A. H. M., Abdul Kadir, K., Tasnim, R., and Fadzil Ismail, A., 2017, "A Capacitive Proximity Sensing Scheme for Human Motion Detection," Proceedings of IEEE International Instrumentation and Measurement Technology Conference (I2MTC), Turin, Italy, May 22–25, pp. 1–5.
[17] Mathiyazhagan, R., Sampathkumar, S., and Muthuramalingam, T., 2019, "Prediction Modeling of Surface Roughness Using Capacitive Sensing Technique in Machining Process," IEEE Sensors J., **19**(21), pp. 9997–10002.
[18] Braun, A., Wichert, R., Kuijper, A., and Fellner, D. W., 2015, "Capacitive Prox-Imity Sensing in Smart Environments," J. Ambient Intell. Smart Environ., **7**(4), pp. 483–510.
[19] Dehkhoda, F., Frounchi, J., and Veladi, H., 2010, "Capacitive Proximity Sensor Design Tool Based on Finite Element Analysis," Sensor Rev., **30**(4), pp. 297–304.
[20] Bryan, J., 1967, "Spindle Accuracy," Am. Mach., **111**(25), pp. 149–164.
[21] Donaldson, R. R., 1972, "A Simple Method for Separating Spindle Error From Test Ball Roundness Error," CIRP, **21**(1), pp. 125–126.
[22] Cogorno, G. R., 2020, *Geometric Dimensioning and Tolerancing for Mechanical Design, 3E. Chapter Form and Appendix*, McGraw-Hill Education, New York.
[23] Krulikowski, A., 2017, Ultimate GD&T Pocket Guide, SAE, 2nd ed., SAE International, US, pp. 53–58.
[24] Proffitt, D., 1982, "The Measurement of Circularity and Ellipticity on a Digital Grid," Pattern Recogn., **15**(5), pp. 383–387.
[25] Kopanja, L., Žunić, D., Lončar, B., yergyek, S., and Tadić, M., 2016, "Quantifying Shapes of Nanoparticles Using Modified Circularity and Ellipticity Measures," Measurement, **92**, pp. 252–263.
[26] Buckrop, L. R., 1963, "Concentricity Determinations for Hollow Cylindrical Shapes Utilizing Resonant Energy," Proc. Iowa Acad. Sci., **70**(1), pp. 391–393.
[27] Smith, P. T., Vallance, R. R., and Marsh, E. R., 2005, "Correcting Capacitive Displacement Measurements in Metrology Applications With Cylindrical Artifacts," Precis. Eng., **29**(3), pp. 324–335.
[28] Capacitec, 2020, Displacement Sensing Systems, https://www.capacitec.com/Displacement-Sensing-Systems/Cylindrical-Probes
[29] Tan, B., Mao, X., Liu, H., Li, B., He, S., Peng, F., and Yin, L., 2014, "A Thermal Error Model for Large Machine Tools That Considers Environmental Thermal Hysteresis Effects," Int. J. Mach. Tools Manuf., **82**, pp. 11–20.